

Oriented Quasi-2D Perovskites for High Performance Optoelectronic Devices

Rong Yang, Renzhi Li, Yu Cao, Yingqiang Wei, Yanfeng Miao, Wen Liang Tan, Xuechen Jiao, Hong Chen, Liangdong Zhang, Qing Chen, Huotian Zhang, Wei Zou, Yuming Wang, Ming Yang, Chang Yi, Nana Wang, Feng Gao, Christopher R. McNeill, Tianshi Qin, Jianpu Wang,* and Wei Huang*

Quasi-2D layered organometal halide perovskites have recently emerged as promising candidates for solar cells, because of their intrinsic stability compared to 3D analogs. However, relatively low power conversion efficiency (PCE) limits the application of 2D layered perovskites in photovoltaics, due to large energy band gap, high exciton binding energy, and poor interlayer charge transport. Here, efficient and water-stable quasi-2D perovskite solar cells with a peak PCE of 18.20% by using 3-bromobenzylammonium iodide are demonstrated. The unencapsulated devices sustain over 82% of their initial efficiency after 2400 h under relative humidity of $\approx 40\%$, and show almost unchanged photovoltaic parameters after immersion into water for 60 s. The robust performance of perovskite solar cells results from the quasi-2D perovskite films with hydrophobic nature and a high degree of electronic order and high crystallinity, which consists of both ordered large-bandgap perovskites with the vertical growth in the bottom region and oriented small-bandgap components in the top region. Moreover, due to the suppressed nonradiative recombination, the unencapsulated photovoltaic devices can work well as light-emitting diodes (LEDs), exhibiting an external quantum efficiency of 3.85% and a long operational lifetime of ≈ 96 h at a high current density of 200 mA cm^{-2} in air.


device stability impedes its commercialization, mainly stemming from the chemical decomposition of regular 3D perovskites in damp environment.^[3,4] Encapsulation techniques can slow down the degradation process, but the essential approach to tackle this issue is to find stable perovskite materials capable of achieving long-term stability.^[5] In contrast to traditional 3D counterparts, quasi-2D layered perovskites have shown enhanced stability owing to the bulkier and hydrophobic organic molecule in the structure, and have been applied both in photovoltaics and light-emitting diodes.^[6–9] Quasi-2D perovskites take the generic structural formula of $\text{L}_2\text{S}_{n-1}\text{M}_n\text{X}_{3n+1}$, where n is an integer, M is a divalent metal, X is a halide anion, and L and S are organic cations with large and small sizes, respectively.^[10] Layered structures are usually formed by inserting the large-sized organic cation spacers into the inorganic sheets of corner-sharing $[\text{MX}_6]$ octahedra. These quasi-2D compounds can be regarded as natural formed quantum-well (QW) structures, in which the semiconducting inorganic sheets act as the wells and the organic dielectric layers correspond to the

Organic–inorganic hybrid perovskite solar cells (PSCs) have undergone rapid development since 2009 with a power conversion efficiency (PCE) of up to 23.2%.^[1,2] However, poor

can be regarded as natural formed quantum-well (QW) structures, in which the semiconducting inorganic sheets act as the wells and the organic dielectric layers correspond to the

R. Yang, Dr. R. Li, Y. Cao, Y. Wei, Y. Miao, H. Chen, L. Zhang, Q. Chen, W. Zou, M. Yang, Dr. C. Yi, Dr. N. Wang, Prof. T. Qin, Prof. J. Wang, Prof. W. Huang
Key Laboratory of Flexible Electronics (KLOFE) & Institute of Advanced Materials (IAM)
Jiangsu National Synergetic Innovation Center for Advanced Materials (SICAM)
Nanjing Tech University (NanjingTech)
30 South Puzhu Road, Nanjing 211816, China
E-mail: iamjpwang@njtech.edu.cn; iamwhuang@nwpu.edu.cn
W. L. Tan, Dr. X. Jiao, Prof. C. R. McNeill
Department of Materials Science and Engineering
Monash University
Wellington Road, Clayton, VIC 3800, Australia

Dr. X. Jiao
Australian Synchrotron (ANSTO)
800 Blackburn Road, Clayton, VIC 3168, Australia
H. Zhang, Y. Wang, Prof. F. Gao
Department of Physics
Chemistry and Biology (IFM)
Linköping University
Linköping SE-58183, Sweden
Prof. W. Huang
Shaanxi Institute of Flexible Electronics (SIFE)
Northwestern Polytechnical University (NPU)
127 West Youyi Road, Xi'an 710072, Shaanxi, China

 The ORCID identification number(s) for the author(s) of this article can be found under <https://doi.org/10.1002/adma.201804771>.

DOI: 10.1002/adma.201804771

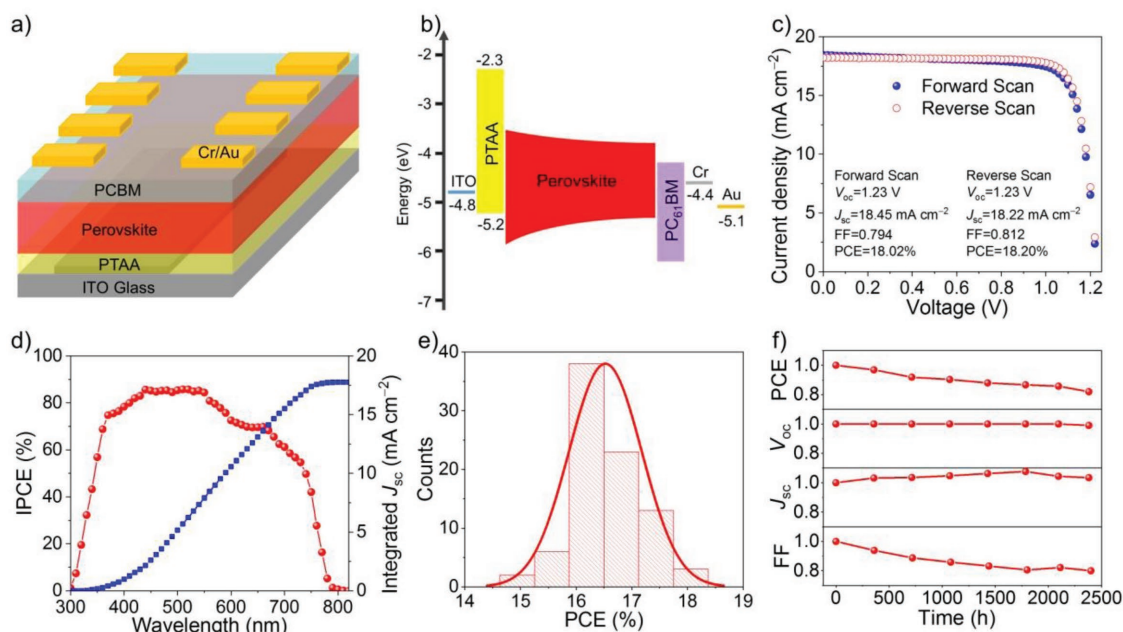


Figure 1. Solar cell architecture and characterization. a) Solar cell architecture. b) Energy level diagram of the quasi-2D perovskite solar cell. The energy level values was taken from the previous report.^[9,23–25] c) J - V curve for the champion cell based on the quasi-2D perovskites. The J - V curves were recorded from the forward sweep (from J_{sc} to V_{oc}) and reverse sweep (from V_{oc} to J_{sc}) under AM1.5G illumination showing negligible hysteresis. d) IPCE spectrum and integrated short circuit current density as a function of wavelength. e) Histogram of solar cell efficiency for 85 devices. The curve is a normal distribution function, illustrating the spread in measured performance. f) Evaluation of photovoltaic parameters of unsealed device which were kept in a dark oven under $\approx 40\%$ relative humidity for 2400 h.

barriers.^[11,12] In recent years, several studies have reported quasi-2D perovskite solar cells mainly based on either i) phenylethylammonium, with the PCEs of 4.73% ($n = 3$)^[6] and 15.3% ($n = 60$)^[13] or ii) butylammonium, with PCEs ranging from 4.02% to 14% ($n = 3$ or 4), and more recently 17.5% with 2D–3D heterostructure.^[7,14–18] In addition, a remarkable PCE of 17.4% has been achieved by using benzylammonium for layered perovskites ($n = 9$).^[19] Although quasi-2D layered perovskites have shown promising stability against moisture, a few challenges need to be addressed in order to achieve high efficiency solar cells, such as poor interlayer charge transport, large energy band gap and high exciton binding energy.^[7,20] Two main strategies have been developed to enhance the device performance of quasi-2D perovskite solar cells.^[21] One is increasing the number (n value) of inorganic sheets between two adjacent organic spacers, although this approach sacrifices stability to some extent.^[13] The other approach is tuning of the crystal growth orientation perpendicular to the substrate to achieve rapid charge transport, however the efficiency is still much lower than that of their 3D counterparts due to the narrower absorption across the solar spectrum and higher exciton binding energy.^[14,22]

Herein, we demonstrate efficient and water-stable perovskite solar cells with a peak PCE of 18.20% by using 3-bromobenzylammonium iodide (3BBAI) based quasi-2D perovskites with good moisture resistance due to its hydrophobic nature. The excellent performance of solar cells stems from the robust quasi-2D perovskite films with high crystallinity and order. Moreover, due to the suppressed nonradiative recombination, the solar cell can be operated as a light-emitting diode (LED),

which shows an external quantum efficiency of 3.85% with better stability than near-infrared organic LEDs.

The devices were fabricated in the inverted planar configuration: indium tin oxide (ITO)/Poly[bis(4-phenyl)-(2,4,6-trimethylphenyl)amine] (PTAA, 30 nm)/perovskite (350 nm)/[6,6]-phenyl-C₆₁-butyric acid methyl ester (PC₆₁BM, 100 nm)/chromium (Cr, 3 nm)/gold (Au, 100 nm), as shown in Figure 1a. The energy-level diagram is shown in Figure 1b, wherein the energy level values for perovskite and PTAA were obtained from the previous reports.^[23–25] In this device structure, PTAA acts as the hole extraction layer and PC₆₁BM as the electron transporting layer. Quasi-2D perovskite films were prepared by using a precursor solution of 3BBAI, methylammonium chloride (MACl), and lead iodide (PbI₂) with a molar ratio of 2:2:3.^[6,14] The content of MACl and 3BBAI reactants was successively adjusted to perform initial efficiency optimization of quasi-2D perovskite solar cells. Figure S1 (Supporting Information) shows the photovoltaic parameters of the various quasi-2D perovskite solar cells under the standard AM1.5G illumination. The devices based on 3BBAI, MACl and PbI₂ with a molar ratio of 1.8:2.5:3 (corresponding to $3 < n < 4$) exhibit an optimized PCE of up to 16.31%. Based on the best molar ratio, we further optimized device performance and recorded the current density–voltage (J - V) curve of the champion cell. The J - V curves presented in Figure 1c were measured with a scanning rate of 0.02 V s^{−1} in both forward- and reverse-scan modes under AM1.5G illumination. Negligible variation of J - V characteristics was observed between the two modes, suggesting almost no hysteresis in our quasi-2D perovskite solar cells. A peak PCE of 18.20% is achieved, mainly due to an extremely

high open-circuit voltage (V_{oc}) of 1.23 V along with a good fill factor (FF) of 0.812, in spite of a relatively low short-circuit current density (J_{sc}) of 18.22 mA cm^{-2} . Incident photon-to-electron conversion efficiency (IPCE) spectrum was carried out to validate the solar simulator measurement of device performance. As displayed in Figure 1d, the IPCE spectrum shows an onset of around 790 nm ($\approx 1\%$ IPCE) and exhibits quantum efficiency value of over 70% from 360 to 660 nm, reaching a maximum of 86% at 510 nm. The integrated J_{sc} from the IPCE spectrum is calculated to be 17.77 mA cm^{-2} , which matches well ($\approx 2.5\%$) the J_{sc} measured under AM1.5G standard irradiation. We prepared 85 cells independently under the same experimental conditions. The histogram of average PCEs (Figure 1e) shows that $\approx 85\%$ of cells had PCEs exceeding 16% under one sun illumination with an average efficiency of $\approx 16.53\%$.

Considering the ubiquitous presence of humidity (from water vapor in air) and water (from rain) in all realistic operating conditions of solar cells, we evaluated the stability of our quasi-2D perovskite devices under the atmospheric humidity and the water-soaking test, respectively. Figure 1f illustrates the evolution of normalized photovoltaic parameters over time for an unencapsulated device, which is stored in a chamber at room temperature with a relative humidity of $\approx 40\%$, and carried out the J - V tests at room temperature in ambient air. The device exhibits robust stability, retaining 82% of its initial efficiency after aging 2400 h. We note that a humidity of $\approx 40\%$

does not decrease the J_{sc} and V_{oc} of the quasi-2D perovskite solar cell, but rather affects the FF. The water-soaking test was further carried out by using a larger device with active area of 0.49 cm^2 . We compared the J - V characteristics before and after immersion in water for 60 s. The pristine device shows a PCE of 12.9% (J_{sc} : 14.42 mA cm^{-2} , V_{oc} : 1.18 V, and FF: 0.760) under one sunlight illumination. Very encouragingly, no efficiency drop was observed in the quasi-2D perovskite device after water immersion, and the J_{sc} (14.16 mA cm^{-2}), V_{oc} (1.18 V), and FF (0.770) remain almost unchanged. The detailed procedures of the water-soaking test are shown in a Movie S1 (Supporting Information). The robust stability of the unsealed large-area device in water represents a major progress in stabilizing the perovskite solar cells against moisture and liquid water.

To reveal the origin of the excellent device performance, we investigated the quality of perovskite films as the photoactive layers. We first investigated the morphology of the quasi-2D perovskite film by scanning electron microscopy (SEM) and atomic force microscope (AFM) measurements. From the top view SEM image in Figure 2a, we observed a full-coverage film with densely packed micrometer-scale crystalline grains. The AFM image (Figure S2, Supporting Information) shows that the quasi-2D perovskite film has very smooth surface with a low root-mean-square roughness (R_{rms}) of $\approx 10.7 \text{ nm}$. The dense and uniform perovskite film suggests that leakage current due to direct contact of PC₆₁BM with PTAA can be minimal. Fourier-transform photocurrent spectroscopy (FTPS) was used

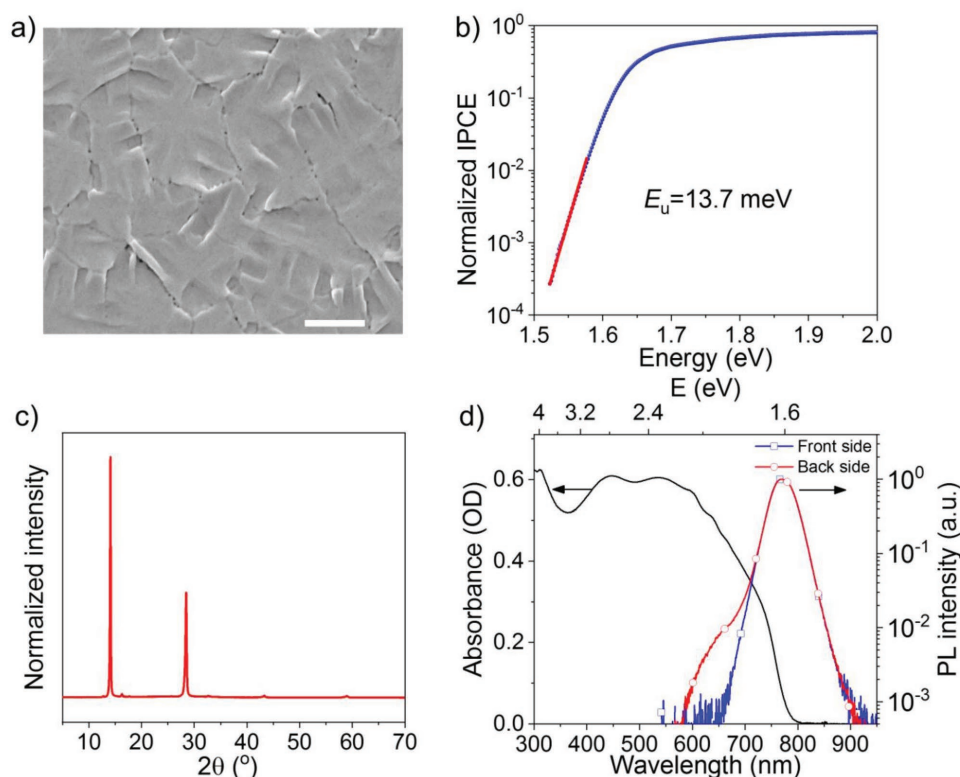


Figure 2. Characterization of quasi-2D perovskite films. a) Top view SEM image of a quasi-2D perovskite film. Scale bar, 1 μm . b) Semilog plot of IPCE at the absorption onset for a quasi-2D perovskite solar cell, measured using FTPS at short-circuit (J_{sc}). An E_u of 13.7 meV can be obtained from the red line. c) X-ray diffraction pattern of a quasi-2D perovskite film on a glass substrate, showing a good crystal orientation. d) Absorption and PL spectra of a quasi-2D perovskite film on a glass substrate. The PL spectra were excited and measured from the front (perovskite side) and back (glass side).

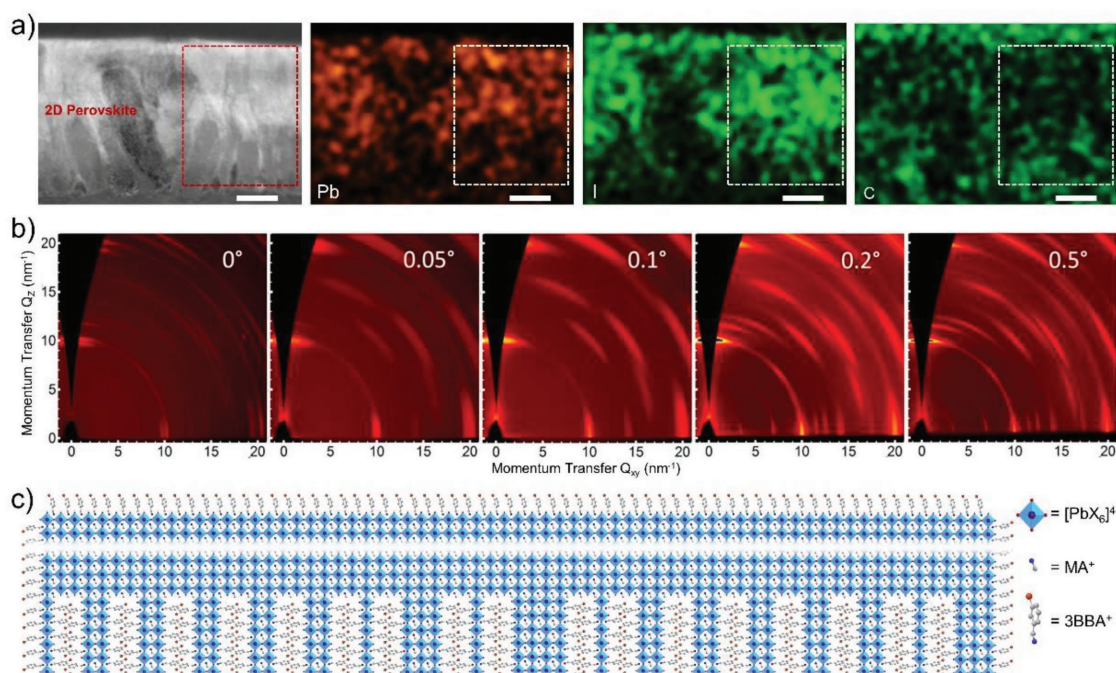


Figure 3. Cross-sectional STEM and EDS images, GIWAXS data, and proposed film structure. a) Cross-sectional STEM image and EDS elemental maps corresponding to the Pb, I, and C of a quasi-2D perovskite film. The scale bar is 100 nm. b) GIWAXS images of a quasi-2D perovskite film. The incidence angles are 0°, 0.05°, 0.1°, 0.2°, and 0.5°. c) Schematic illustration of the proposed self-assembled quasi-2D perovskite film structure.

to determine the Urbach energy (E_u), which can quantify the electronic disorder of the quasi-2D perovskite films.^[26] The semilog plot of IPCE onset of a high efficiency device is depicted in Figure 2b, showing a sharp absorption edge and therefore an E_u of 13.7 meV. This E_u is fairly low in values reported for high quality lead halide perovskites, indicating a high degree of electronic order in our quasi-2D perovskite films.^[27–29] We further investigated the crystallinity of the perovskite film by X-ray diffraction (XRD) (Figure 2c). The XRD pattern shows two dominant diffraction peaks at 14.14° and 28.50°, which indicate that the quasi-2D perovskite film possesses large crystal size and highly oriented crystal structure, agreeing well with the results of SEM and FTPS measurements. We further studied the light-harvesting ability of quasi-2D perovskite films, which is an important factor affecting IPCE and photocurrent. As depicted in Figure 2d, the quasi-2D perovskite film exhibits a wide absorption range up to ≈ 800 nm, which is beneficial for the utilization of low-energy solar photons. In the range between 400 and 700 nm, additional exciton absorption peaks stemming from the small n components are clearly observed, confirming that our quasi-2D perovskite film has mixed-dimensional components.^[6,9,12,30] To study the uniformity of the film, the PL spectra are measured under two excitation configurations of the front (perovskite side) and back (glass side). As shown in Figure 2d, the front excitation leads to a Gaussian symmetrical PL peak at 768 nm, while the back excitation causes the extra PL emission in the range between 620 and 700 nm. The PL difference of the two excitation configurations suggests that in the quasi-2D perovskite film the large n components are mainly located at the upper surface of the film, and the small n components remains at the bottom (glass) side.^[16,31]

To further investigate the film structure, we firstly analyzed a cross-sectional quasi-2D perovskite film by an aberration-corrected scanning transmission electron microscope (STEM). The contrast of high-angle annular dark-field (HAADF) STEM image shows that the perovskite film is constructed of two parts (Figure 3a). At the bottom region of the film, perovskite grains with more than 100 nm length grow along the direction perpendicular to the substrate. The ≈ 180 nm thick, smooth and pinhole-free perovskite layer with few grain boundaries covers the top of vertical-oriented crystalline grains, which is consistent with the observation of XRD and the surface-view SEM images. Energy-dispersive X-ray spectroscopy (EDS) maps are shown in Figure 3a to determine the content and distribution of the elements lead, iodine and carbon in the perovskite film. Compared to the bottom region, the top area of the perovskite film shows stronger signals of both lead and iodine but weaker signals of carbon. The inhomogeneous distribution of lead, iodine and carbon across the perovskite film suggests that the [PbI₆] octahedra units distribute more in the top layer and organic cation units are localized more in the bottom layer.^[9] Grazing-incidence wide-angle X-ray scattering (GIWAXS) measurement was also performed to further probe the crystallography structure of the perovskite film. GIWAXS measurements were performed as a function of angle of incidence, α , which can provide depth-sensitive information provided the layers are uniform enough (which is the case for the films prepared here). For angles below the critical angle ($\alpha < 0.2^\circ$) where the X-rays penetrate only the top 10 nm of the film or so, the 2D scattering patterns resemble that of highly textured 3D-like (large n) perovskite, with all peaks matching those seen in a 3D material. For angles of $\alpha = 0.2^\circ$ and 0.5° for which the X-ray beam penetrates fully

into the film, additional peaks appear which are indicative of a highly ordered and oriented 2D phase (small n). In particular peaks at $q = 3.5 \text{ nm}^{-1}$ and $q = 7.0 \text{ nm}^{-1}$ are observed along the in-plane scattering direction which can be assigned to (020) and (040) reflections of $n = 2$ 2D perovskite.^[7,32] The appearance of these peaks along the q_{xy} direction and not the q_z direction supports the vertical orientation of small- n components, which is consistent with the STEM measurement results. The observation of peaks which are characteristic of 2D layered perovskite features is also significant since previous reports of 2D perovskite thin films have shown GIWAXS patterns that exhibit only 3D-like features,^[14,33,34] suggesting that the small- n ordering in such materials may be rather disordered, lacking the period layering of small- n components. Indeed, while other orders are apparent in our sample based on the optical analysis, only the $n = 2$ perovskite exhibits periodic ordering. In general the 2D GIWAXS data are consistent with the XRD shown in Figure 2c, where the dominant peaks at 14.14° and 28.50° match the main peaks which are indexed as (110) and (220) for 3D-like (large- n) perovskites or as (111) and (202) for small- n components.^[7,14,34] However, due to the highly textured nature of these films the lab-based XRD measurements which only probe out-of-plane scattering miss the key 2D peaks that appear in-plane, as reported in the literature.^[7]

The above information allows us to form a clear understanding of the unique structure of our quasi-2D perovskite films, as illustrated in Figure 3c. Although the mechanism is not clear, the introduction of 3BBAI actually induces the oriented growth of small- n perovskites perpendicular to the substrate, following by the order crystallization of large- n components at top. The large- n components with high crystallinity in the upper region are advantageous for low-energy solar photon capture and exciton dissociation due to narrow energy gap and small exciton binding energy. Moreover, the large- n perovskites form smooth and continuous film surface, minimizing the leakage current of the device. The small- n components with vertical orientation in the lower region facilitate the rapid transport of photogenerated carriers across the perovskite films, following by efficient extraction of hole or electron transport layers, respectively.^[7,14] Therefore, our quasi-2D perovskite solar cell show a wide and high IPCE spectrum, as well as a high FF.

To further understand the origin of our robust device performance, we compared quasi-2D perovskite films and devices based on benzylammonium iodide (BAI) and 3BBAI. Figure S3 (Supporting Information) exhibits the SEM images of the quasi-2D perovskite films made from BAI and 3BBAI. Two films show the densely packed micrometer-scale crystalline grains. However, the BAI perovskite film has pinholes and the 3BBAI counterpart does not, indicating that 3BBAI compared to BAI can improve the morphology of quasi-2D perovskite films. GIWAXS data analysis of the BAI perovskite film (Figure S4, Supporting Information) suggest a similar layered structure with characteristic 2D peaks again appearing at higher values of α . The low- q 2D peaks appear at slightly higher q values ($q = 3.8 \text{ nm}^{-1}$, 7.5 nm^{-1}) consistent with the slightly smaller spacing between 2D sheets. The BAI perovskite film shows again a large degree of texture, but with the presence of a population of large- n crystallites that are randomly

oriented indicated by the coexistence of isotropic rings and well-defined peaks. The film stability was examined by exposing the quasi-2D perovskite films to a high relative humidity level of 90% and recording their XRD data (Figure S5, Supporting Information). Upon humidity exposure for 10 min, the XRD pattern of the BAI perovskite film shows an obvious PbI_2 diffraction peak, but the 3BBAI perovskite film still illustrates an unchanged XRD pattern even after 60 min, indicating its outstanding stability against moisture. We believe that the halogen substituent of 3-bromobenzylammonium iodide plays a key role in improving the stability of our perovskite films, presumably due to its hydrophobic nature and the film with pinhole-free morphology and good crystallinity. The UV-vis absorption spectra in Figure S6 (Supporting Information) show that the light absorption of the 3BBAI perovskite film in the range of 300–800 nm is slightly weaker than that of the BAI counterpart, but the overall absorption difference is not significant. We further investigated the photovoltaic performance of quasi-2D perovskite solar cells made from BAI and 3BBAI, respectively. As shown in Table S1 (Supporting Information), the 3BBAI-based devices show greater performance than the BAI-based devices. We note that the BAI devices based on BAI, MACl, and PbI_2 with molar ratio of 2:2:3 and 2:3:4 exhibit 11.50% and 13.33% average efficiency, respectively, which are comparable to that reported in the literature.^[14]

Importantly, the high quality quasi-2D perovskite film with unique structure not only enhance FF and J_{sc} , but also make an important contribution to the high V_{oc} of our devices due to minimization of nonradiative recombination processes. We quantified the nonradiative recombination losses according to the external quantum efficiency (EQE_{EL}) of electroluminescence (EL) by operating a solar cell as a LED.^[35–37] Figure 4a depicts the relationship of both current density and radiance with voltage for the perovskite LED with a low turn-on voltage of 1.25 V. The near-infrared EL emission peaked at $\approx 760 \text{ nm}$ is also shown in the inset of Figure 4a. The current density and EL increase rapidly along with the bias voltage, implying good charge transport of the quasi-2D perovskite film. A peak brightness of $192.1 \text{ W sr}^{-1} \text{ m}^{-2}$ is obtained under a driving voltage of 2.85 V, which is comparable to the highest radiance of the reported near-infrared (NIR) perovskite LED.^[38] As shown in the inset of Figure 4b, the EQE_{EL} of $\approx 1.5\%$ is chosen at an injection current that is equal to the photocurrent of 18.22 mA cm^{-2} . We estimate the nonradiative losses ($\Delta V_{\text{oc,nonrad}}$) of the photovoltage according to the formula^[36]

$$\Delta V_{\text{oc,nonrad}} = \frac{kT}{e} \ln \text{EQE}_{\text{EL}} \quad (1)$$

where k is Boltzmann constant, T is the temperature, and e is the elementary charge. The $\Delta V_{\text{oc,nonrad}}$ is calculated to be $\approx 0.11 \text{ V}$, which is one of the lowest reported values in perovskite solar cells.^[37] The low $\Delta V_{\text{oc,nonrad}}$ for our device indicates that the quasi-2D perovskite film has very low bulk and surface defect density and all major sources of nonradiative recombination are strongly suppressed. By the integration of the IPCE over the blackbody radiation and AM1.5G solar spectra, we estimate the theoretical radiative limit ($V_{\text{oc,rad}}$) of the photovoltage to be $\approx 1.35 \text{ V}$.^[36,39] According to calculated values of $V_{\text{oc,rad}}$ and

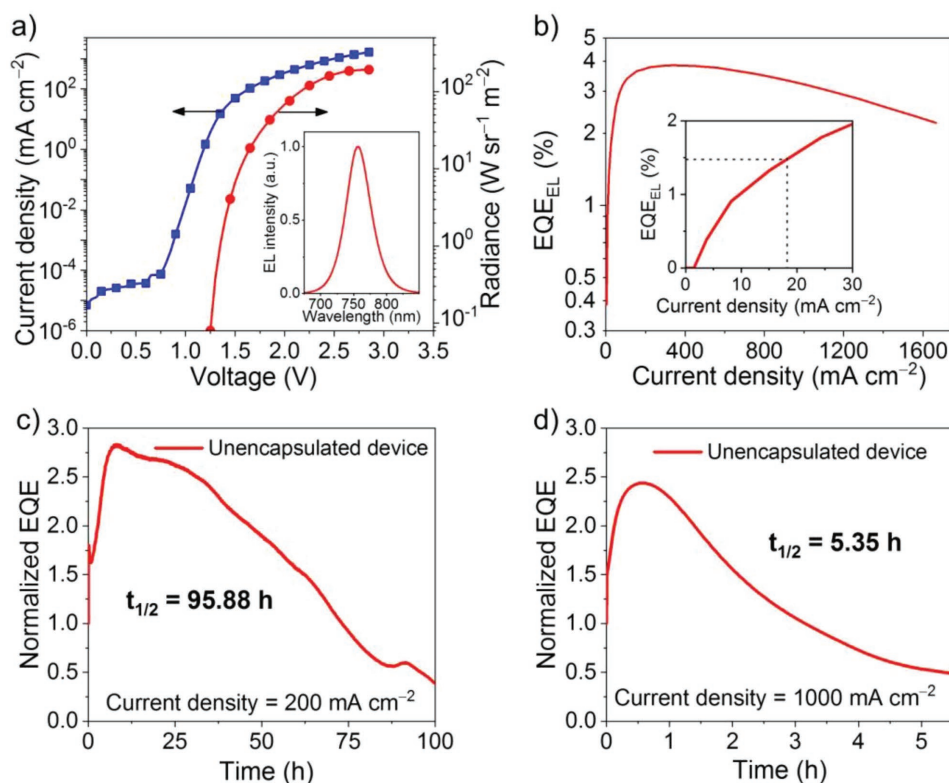


Figure 4. Optoelectronic properties of quasi-2D perovskite solar cells measured as LED devices. a) Plots of current density and radiance versus driving voltage. Inset shows the corresponding electroluminescence (EL) spectrum at 2.5 V. b) Plot of external electroluminescence quantum efficiency (EQE_{EL}) versus current density. Inset shows the EQE_{EL} of ≈1.5% at a driving current equal to the short-circuit current of the device. Evolution of the EQE_{EL} for the unencapsulated quasi-2D perovskite LED measured under an air atmosphere of ≈37% RH at a constant current density of c) 200 mA cm⁻² and d) 1000 mA cm⁻².

$\Delta V_{oc, nonrad}$, a predicted V_{oc} of 1.24 V is obtained, confirming the value of 1.23 V measured from the $J-V$ curve.

Furthermore, the EQE_{EL} of the solar cell device reaches up to 3.85% at a high current density of 342 mA cm⁻² (Figure 4b) and a high brightness of 68.4 W sr⁻¹ m⁻² (Figure 4a). The quasi-2D perovskite LED shows a low efficiency roll-off at high driving current density. The EQE_{EL} value has almost no roll-off at 500 mA cm⁻² and remains 50% of its peak even at an enormous injection current density of 1880 mA cm⁻². We evaluate the operation stability of the unencapsulated LED devices under an air atmosphere with relative humidity of ≈37%. As shown in Figure 4c,d, an enhancement of the EQE_{EL} can be observed in the first few hours of device operation. We believe this is probably resulting from two reasons: 1) a slow trap-filling process by the injected carriers and/or ionic motion; 2) a slow internal field-redistribution due to local ionic motion of excess ions under external electric field.^[40,41] The device EQE_{EL} decays to half of the initial value after ≈96 h of continuous operation at a given current density of 200 mA cm⁻², creating a new record of operation lifetime for perovskite LEDs, and even better than the best performing near infrared organic LEDs.^[9,42–44] For a higher injection current density of 1000 mA cm⁻², the operation lifetime of quasi-2D perovskite LED still reaches an impressed 5.35 h. Our results suggest that the good stability of the LED devices can be attributed to the intrinsic stability of quasi-2D perovskite films with high crystallinity and a low level of defects.

In summary, we have demonstrated that high performance solar cells and LEDs can be achieved by using 3BBAI based quasi-2D perovskite film. The film has a layered structure of vertically oriented small-*n* perovskites covered by a layer of oriented large-*n* components. This unique microstructure leads to form an energetically ordered and highly crystalline perovskite film with good charge transport, suppressed nonradiative recombination, and excellent moisture resistance. Our results suggest that 3BBAI based quasi-2D perovskite materials are ideal for highly efficient and stable perovskite solar cell, LEDs and other optoelectronic applications, and tuning the growth of 2D perovskite films is a key step toward achieving this goal.

Experimental Section

Synthesis and Materials Preparation: 3BBAI was synthesized by adding hydroiodic acid (1 mmol) into a solution of *m*-Br-benzylamine (1 mmol) in ethanol (20 mL) at 0 °C and then stirred for 2 h. Next, the solution was evaporated at 60 °C to obtain precipitates, which were washed three times with diethyl ether and then vacuum-dried at 35 °C for 12 h. Precursor solution were prepared by dissolving 3BBAI, MAI, and PbI₂ in DMF with different molar ratio in DMF at a weight concentration of 20% and stirring at 60 °C for 8 h in a nitrogen-filled glovebox.

Device Fabrication: ITO-coated glass substrates were cleaned sequentially in acetone and alcohol, followed by 10 min oxygen plasma treatment. The substrates were transferred into a nitrogen-filled glove box for the further fabrication steps. A hole-transport layer of PTAA

(molecular weight: 1000–10 000 g mol⁻¹) from a chlorobenzene solution (6 mg mL⁻¹) was spin-coated onto the indium tin oxide (ITO) substrate at 5000 rpm for 30 s and annealed at 100 °C for 10 min. After the substrates were heated to a temperature of 140 °C, the perovskite films were deposited by hot-casting the precursor solution onto the substrates at 5000 rpm for 20 s and annealed at 90 °C for 15 min. An electron-transport layer of PC₆₁BM was deposited from a chlorobenzene solution (20 mg mL⁻¹) at 1000 rpm for 60 s. Finally, the Cr and Au layers were deposited using a thermal evaporation system through a shadow mask under a base pressure of $\approx 6 \times 10^{-7}$ Torr. The device area was 0.03 cm² as defined by the overlapping area of the ITO film and top electrode.

Device Characterization: All perovskite solar cells were measured under simulated AM1.5 G irradiation at 100 mW cm⁻² by using a solar simulator (Class AAA, SS-F5-3A, Enlitech) and current–voltage curves were recorded by a Keithley 2450 source meter. The light intensity was calibrated by using a Newport standard silicon cell 91150. The devices were swept from zero bias to forward bias with scan rate of 0.02 V s⁻¹. IPCE measurements were carried out in DC mode by using a Keithley 2400 source meter and a SOFN 71SW752 monochromator equipped with a 500 W Xenon lamp. The wavelength sampling interval was 10 nm and the current sampling time was 1 s, which was fully controlled by computer. A Hamamatsu S1337-1010BQ silicon diode used for IPCE measurements was calibrated at the National Institute of Metrology, China. For LED device characterizations, a Keithley 2400 source meter was used for J–V measurement and a fiber integration sphere (FOIS-1) couple with a QE65 Pro spectrometer was used for the light output measurement.

Film Characterization: The absorbance spectra were measured by a UV–vis spectrophotometer with an integrating sphere (PerkinElmer, Lambda 950). The PL spectra were measured by using a QE65 Pro spectrometer and a 445 nm CW laser as an excitation source. XRD data were obtained by using a Bruker D8 Advance. The STEM image of cross-sectional device was collected on a FEI Titan G2 80-200 ChemiSTEM operated at 200 keV. The HRTEM image was collected on a Tecnai G2 F20 microscope operated at 200 keV. Element determinations were obtained by ChemiSTEM EDX system. The SEM images of perovskite films were obtained by using a JEOL5 JSM-7800F SEM. The surface morphology of perovskite film was collected by AFM (Bruker, Dimension Icon SPM). GIWAXS measurements were performed at the SAXS/WAXS beamline at the Australian Synchrotron.^[45] 12 keV photons were used, with 2D scattering patterns recorded on a Dectris Pilatus 1M detector. A sample to detector distance of ≈ 34.1 cm was used, with the sample-to-detector distance calibrated with a silver behenate sample. Exposure times of 1 s were used, with a fresh spot used for each different angle to avoid beam damage.

Supporting Information

Supporting Information is available from the Wiley Online Library or from the author.

Acknowledgements

R.Y. and R.L. contributed equally to this work. The authors would like to acknowledge the funding from the National Basic Research Program of China-Fundamental Studies of Perovskite Solar Cells (2015CB932200), the Joint Research Program between China and European Union (2016YFE0112000), Major Research Plan of the National Natural Science Foundation of China (91733302), the National Key Research and Development Program of China (2018YFB0406704 and 2017YFB0404500), the Natural Science Foundation of Jiangsu Province, China (BK20150043, BK20170991, and BK20150064), Major Program of Natural Science Research of Jiangsu Higher Education Institutions of China (18KJA510002), the National Natural Science Foundation of China (61634001, 51703094,

and 11474164), the National Science Fund for Distinguished Young Scholars (61725502), and the Synergetic Innovation Center for Organic Electronics and Information Displays.

Conflict of Interest

The authors declare no conflict of interest.

Keywords

multiple quantum wells, perovskites, solar cells, stability, two dimension

Received: July 25, 2018
Revised: September 24, 2018
Published online: October 21, 2018

- [1] A. Kojima, K. Teshima, Y. Shirai, T. Miyasaka, *J. Am. Chem. Soc.* **2009**, *131*, 6050.
- [2] N. J. Jeon, H. Na, E. H. Jung, T.-Y. Yang, Y. G. Lee, G. Kim, H.-W. Shin, S. I. Seok, J. Lee, J. Seo, *Nat. Energy* **2018**, *3*, 682.
- [3] E. Mosconi, J. M. Azpiroz, F. De Angelis, *Chem. Mater.* **2015**, *27*, 4885.
- [4] Z. Song, A. Abate, S. C. Watthage, G. K. Liyanage, A. B. Phillips, U. Steiner, M. Graetzel, M. J. Heben, *Adv. Energy Mater.* **2016**, *6*, 1600846.
- [5] Y. Han, S. Meyer, Y. Dkhissi, K. Weber, J. M. Pringle, U. Bach, L. Spiccia, Y.-B. Cheng, *J. Mater. Chem. A* **2015**, *3*, 8139.
- [6] I. C. Smith, E. T. Hoke, D. Solis-Ibarra, M. D. McGehee, H. I. Karunadasa, *Angew. Chem., Int. Ed.* **2014**, *53*, 11232.
- [7] D. H. Cao, C. C. Stoumpos, O. K. Farha, J. T. Hupp, M. G. Kanatzidis, *J. Am. Chem. Soc.* **2015**, *137*, 7843.
- [8] M. Yuan, L. N. Quan, R. Comin, G. Walters, R. Sabatini, O. Voznyy, S. Hoogland, Y. Zhao, E. M. Beauregard, P. Kanjanaboos, Z. Lu, D. H. Kim, E. H. Sargent, *Nat. Nanotechnol.* **2016**, *11*, 872.
- [9] N. Wang, L. Cheng, R. Ge, S. Zhang, Y. Miao, W. Zou, C. Yi, Y. Sun, Y. Cao, R. Yang, Y. Wei, Q. Guo, Y. Ke, M. Yu, Y. Jin, Y. Liu, Q. Ding, D. Di, L. Yang, G. Xing, H. Tian, C. Jin, F. Gao, R. H. Friend, J. Wang, W. Huang, *Nat. Photonics* **2016**, *10*, 699.
- [10] D. B. Mitzi, C. A. Feild, W. T. A. Harrison, A. M. Guloy, *Nature* **1994**, *369*, 467.
- [11] E. A. Muljarov, S. G. Tikhodeev, N. A. Gippius, T. Ishihara, *Phys. Rev. B* **1995**, *51*, 14370.
- [12] K. Tanaka, T. Kondo, *Sci. Technol. Adv. Mater.* **2003**, *4*, 599.
- [13] L. N. Quan, M. Yuan, R. Comin, O. Voznyy, E. M. Beauregard, S. Hoogland, A. Buin, A. R. Kirmani, K. Zhao, A. Amassian, D. H. Kim, E. H. Sargent, *J. Am. Chem. Soc.* **2016**, *138*, 2649.
- [14] H. Tsai, W. Nie, J.-C. Blancon, C. C. Stoumpos, R. Asadpour, B. Harutyunyan, A. J. Neukirch, R. Verduzco, J. J. Crochet, S. Tretiak, L. Pedesseau, J. Even, M. A. Alam, G. Gupta, J. Lou, P. M. Ajayan, M. J. Bedzyk, M. G. Kanatzidis, A. D. Mohite, *Nature* **2016**, *536*, 312.
- [15] X. Zhang, X. Ren, B. Liu, R. Munir, X. Zhu, D. Yang, J. Li, Y. Liu, D.-M. Smilgies, R. Li, Z. Yang, T. Niu, X. Wang, A. Amassian, K. Zhao, S. Liu, *Energy Environ. Sci.* **2017**, *10*, 2095.
- [16] N. Zhou, Y. Shen, L. Li, S. Tan, N. Liu, G. Zheng, Q. Chen, H. Zhou, *J. Am. Chem. Soc.* **2018**, *140*, 459.
- [17] H. Tsai, R. Asadpour, J.-C. Blancon, C. C. Stoumpos, J. Even, P. M. Ajayan, M. G. Kanatzidis, M. A. Alam, A. D. Mohite, W. Nie, *Nat. Commun.* **2018**, *9*, 2130.

- [18] Z. Wang, Q. Lin, F. P. Chmiel, N. Sakai, L. M. Herz, H. J. Snaith, *Nat. Energy* **2017**, 2, 17135.
- [19] H. Zheng, G. Liu, L. Zhu, J. Ye, X. Zhang, A. Alsaedi, T. Hayat, X. Pan, S. Dai, *Adv. Energy Mater.* **2018**, 8, 1800051.
- [20] B. Saparov, D. B. Mitzi, *Chem. Rev.* **2016**, 116, 4558.
- [21] L. Etgar, *Energy Environ. Sci.* **2018**, 11, 234.
- [22] J.-W. Xiao, L. Liu, D. Zhang, N. De Marco, J.-W. Lee, O. Lin, Q. Chen, Y. Yang, *Adv. Energy Mater.* **2017**, 7, 1700491.
- [23] R. Li, C. Yi, R. Ge, W. Zou, L. Cheng, N. Wang, J. Wang, W. Huang, *Appl. Phys. Lett.* **2016**, 109, 151101.
- [24] J. H. Heo, S. H. Im, J. H. Noh, T. N. Mandal, C.-S. Lim, J. A. Chang, Y. H. Lee, H.-j. Kim, A. Sarkar, M. K. Nazeeruddin, M. Grätzel, S. I. Seok, *Nat. Photonics* **2013**, 7, 486.
- [25] J. Wang, N. Wang, Y. Jin, J. Si, Z.-K. Tan, H. Du, L. Cheng, X. Dai, S. Bai, H. He, Z. Ye, M. L. Lai, R. H. Friend, W. Huang, *Adv. Mater.* **2015**, 27, 2311.
- [26] D. P. McMeekin, G. Sadoughi, W. Rehman, G. E. Eperon, M. Saliba, M. T. Höerantner, A. Haghighirad, N. Sakai, L. Korte, B. Rech, M. B. Johnston, L. M. Herz, H. J. Snaith, *Science* **2016**, 351, 151.
- [27] S. De Wolf, J. Holovsky, S.-J. Moon, P. Löper, B. Niesen, M. Ledinsky, F.-J. Haug, J.-H. Yum, C. Ballif, *J. Phys. Chem. Lett.* **2014**, 5, 1035.
- [28] W. Zhang, S. Pathak, N. Sakai, T. Stergiopoulos, P. K. Nayak, N. K. Noel, A. A. Haghighirad, V. M. Burlakov, D. W. deQuilettes, A. Sadhanala, W. Li, L. Wang, D. S. Ginger, R. H. Friend, H. J. Snaith, *Nat. Commun.* **2015**, 6, 10030.
- [29] J. T.-W. Wang, Z. Wang, S. Pathak, W. Zhang, D. W. deQuilettes, F. Wisnivesky-Rocca-Rivarola, J. Huang, P. K. Nayak, J. B. Patel, H. A. Mohd Yusof, Y. Vaynzof, R. Zhu, I. Ramirez, J. Zhang, C. Ducati, C. Grovenor, M. B. Johnston, D. S. Ginger, R. J. Nicholas, H. J. Snaith, *Energy Environ. Sci.* **2016**, 9, 2892.
- [30] Y. Sun, L. Zhang, N. Wang, S. Zhang, Y. Cao, Y. Miao, M. Xu, H. Zhang, H. Li, C. Yi, J. Wang, W. Huang, *npj Flexible Electron.* **2018**, 2, 12.
- [31] J. Qing, X.-K. Liu, M. Li, F. Liu, Z. Yuan, E. Tiukalova, Z. Yan, M. Duchamp, S. Chen, Y. Wang, S. Bai, J.-M. Liu, H. J. Snaith, C.-S. Lee, T. C. Sum, F. Gao, *Adv. Energy Mater.* **2018**, 8, 1800185.
- [32] C. C. Stoumpos, D. H. Cao, D. J. Clark, J. Young, J. M. Rondinelli, J. I. Jang, J. T. Hupp, M. G. Kanatzidis, *Chem. Mater.* **2016**, 28, 2852.
- [33] T. M. Koh, V. Shanmugam, J. Schlipf, L. Oesinghaus, P. Müller-Buschbaum, N. Ramakrishnan, V. Swamy, N. Mathews, P. P. Boix, S. G. Mhaisalkar, *Adv. Mater.* **2016**, 28, 3653.
- [34] C. M. M. Soe, W. Nie, C. C. Stoumpos, H. Tsai, J.-C. Blancon, F. Liu, J. Even, T. J. Marks, A. D. Mohite, M. G. Kanatzidis, *Adv. Energy Mater.* **2018**, 8, 1700979.
- [35] K. Tvingstedt, O. Malinkiewicz, A. Baumann, C. Deibel, H. J. Snaith, V. Dyakonov, H. J. Bolink, *Sci. Rep.* **2015**, 4, 6071.
- [36] U. Rau, *Phys. Rev. B* **2007**, 76, 085303.
- [37] M. Saliba, T. Matsui, K. Domanski, J.-Y. Seo, A. Ummadisingu, S. M. Zakeeruddin, J.-P. Correa-Baena, W. R. Tress, A. Abate, A. Hagfeldt, M. Grätzel, *Science* **2016**, 354, 206.
- [38] W. Zou, R. Li, S. Zhang, Y. Liu, N. Wang, Y. Cao, Y. Miao, M. Xu, Q. Guo, D. Di, L. Zhang, C. Yi, F. Gao, R. H. Friend, J. Wang, W. Huang, *Nat. Commun.* **2018**, 9, 608.
- [39] W. Tress, N. Marinova, O. Inganäs, M. K. Nazeeruddin, S. M. Zakeeruddin, M. Graetzel, *Adv. Energy Mater.* **2015**, 5, 1400812.
- [40] Z. Xiao, R. A. Kerner, L. Zhao, N. L. Tran, K. M. Lee, T.-W. Koh, G. D. Scholes, B. P. Rand, *Nat. Photonics* **2017**, 11, 108.
- [41] L. Zhao, J. Gao, Y. L. Lin, Y.-W. Yeh, K. M. Lee, N. Yao, Y.-L. Loo, B. P. Rand, *Adv. Mater.* **2017**, 29, 1605317.
- [42] S. Zhang, C. Yi, N. Wang, Y. Sun, W. Zou, Y. Wei, Y. Cao, Y. Miao, R. Li, Y. Yin, N. Zhao, J. Wang, W. Huang, *Adv. Mater.* **2017**, 29, 1606600.
- [43] H. Tsai, W. Nie, J.-C. Blancon, C. C. Stoumpos, C. M. M. Soe, J. Yoo, J. Crochet, S. Tretiak, J. Even, A. Sadhanala, G. Azzellino, R. Brenes, P. M. Ajayan, V. Bulovi, S. D. Stranks, R. H. Friend, M. G. Kanatzidis, A. D. Mohite, *Adv. Mater.* **2018**, 30, 1704217.
- [44] M. Yang, N. Wang, S. Zhang, W. Zou, Y. He, Y. Wei, M. Xu, J. Wang, W. Huang, *J. Phys. Chem. Lett.* **2018**, 9, 2038.
- [45] N. M. Kirby, S. T. Mudie, A. M. Hawley, D. J. Cookson, H. D. T. Mertens, N. Cowieson, V. Samardzic-Boban, *J. Appl. Crystallogr.* **2013**, 46, 1670.